J Mater Sci (2011) 46:174–182
DOI 10.1007/s10853-010-4902-9

Predicting long-term creep failure of bimodal polyethylene pipe from short-term fatigue tests

Zheng Zhou · Anne Hiltner · Eric Baer

Received: 23 June 2010 / Accepted: 4 September 2010 / Published online: 7 October 2010

Abstract Short-term fatigue testing was used to predict long-term creep failure of a bimodal polyethylene (BMPE) pipe with superior creep resistance. The stepwise crack propagation was studied by increasing the R-ratio (defined as the ratio of the minimum to the maximum stress intensity factor in the fatigue loading cycle) at 50 °C from 0.1 approaching creep ($R = 1$). Crack growth rate (da/dt) was related to the maximum stress intensity factor $K_{I,max}$ and R-ratio by a power law relationship $\frac{da}{dt} = B' K_{I,max}^4 (1+R)^{-8.5}$. The correlation in crack growth kinetics allowed for extrapolation to creep fracture from short-term fatigue testing. The temperature dependence of crack growth rate was contained in the prefactor B'. A change in slope of the Arrhenius plot of B' at 67 °C indicated that at least two mechanisms contributed to crack propagation, each dominating in a different temperature region. This implied that a simple extrapolation to ambient temperature creep fracture from elevated temperature tests might not be reliable.

Introduction

The so-called third generation of polyethylene pipe resins provides exceptional improvements in environmental stress crack resistance, resistance to rapid crack propagation and creep resistance compared to earlier generations. The enhanced performance derives from the molecular architecture of the new resins. The structural origin of the polyethylene fracture toughness is thought to reside in the tie molecules [1, 2]. The processes of tie molecule disentanglement and pullout that lead to fracture are severely hampered by incorporation of short chain branches (SCBs) [3, 4]. However, in conventional polyethylenes, the SCB content decreases with molecular weight. The SCBs are concentrated in the chains that are least likely to serve as tie molecules. The new resins with bimodal molecular weight distribution redistribute the SCBs to the high molecular weight chains. The SCBs retard disentanglement and pullout of the tie molecules and increase the topological disorder at the crystal lamella surface. The low molecular weight chains are essentially homopolymer. They provide crystalline anchors for the branched tie molecules. The ratio of the high weight average molecular weight chains to the low weight average molecular weight chains (M_{wH}/M_{wL}) is 30 or more [5].

The superior creep resistance of BMPE challenges the accelerated tests that are used to predict long-term behavior. The PENT test (ASTM F1473) is an elevated temperature test (80 °C) that is designed specifically for predicting the long-term failure of polyethylene natural gas pipe resins [6–8]. However, some of the BMPE resins are reported to have failure times longer than 10,000 h (>1 year) in the PENT test [9].

Short-term fatigue testing is another approach to predicting long-term creep performance [10–12]. To accurately predict long-term failure, the creep failure mechanism must be maintained in fatigue while the crack growth rate is substantially enhanced. Tests in which the stepwise crack propagation mode observed in creep is conserved in fatigue show that the failure time at ambient

Z. Zhou · A. Hiltner · E. Baer (✉)
Department of Macromolecular Science and Engineering,
Case Western Reserve University, Cleveland,
OH 44106-7202, USA
e-mail: exb6@case.edu

Z. Zhou
e-mail: zxz33@case.edu

A. Hiltner
e-mail: ahiltner@case.edu

temperature is up to three orders of magnitude shorter in fatigue compared to creep [4, 13].

The relationship between fatigue and creep is quantitatively examined by systematically decreasing the dynamic component of fatigue loading. This is accomplished by varying the R-ratio (the ratio of $K_{I,min}$, the minimum stress intensity factor, to $K_{I,max}$, the maximum stress intensity factor) so that R gradually approaches unity (creep loading). It is convenient to vary the R-ratio under conditions of constant mean stress intensity factor $K_{I,mean}$ or constant $K_{I,max}$. This approach was previously used to examine the relationship between fatigue and creep in high density polyethylene (HDPE) [14], and in a medium density polyethylene (MDPE) pipe [15]. Stepwise crack propagation was observed in tests under fatigue and creep, and a power law relation described crack growth rate over the entire range of fatigue and creep loading conditions studied

$$\frac{da}{dt} = B' K_{I,max}^{m} (1 + R)^{n} \quad (1)$$

where $m = 4$ for polyethylene and the prefactor B' and the power n vary depending on the specific resin. In creep ($K_I = K_{I,max}$ and $R = 1$), Eq. 1 reduces the conventional Paris relation for creep

$$\frac{da}{dt} = B K_I^{m} \quad (2)$$

where $B = 2^n B'$. Correspondence between the values of B obtained from fatigue (Eq. 1) and the values obtained directly from creep (Eq. 2) for HDPE at ambient temperature [14, 16], and MDPE at 50 °C [17], confirm that short-term fatigue testing can be used to predict long-term creep failure.

The goal of this investigation is to extend the fatigue approach given by Eq. 1 to predict the creep lifetime of a BMPE pipe material. Due to the superior creep resistance of BMPE, an elevated temperature of 50 °C is used. The temperature dependence of fatigue crack growth is also studied in order to predict the lifetime at ambient temperature. Comparisons are made with the previous studies of HDPE and MDPE.

Materials and methods

Specimens

A gas transportation pipe with a outwall diameter of 32 cm was obtained from the Silver-Line Plastic Pipe Company. The pipe had a wall thickness of 30 mm and a wall thickness to diameter ratio of about 11. The pipe was extruded from carbon black-filled (<4 wt%) DOW Continuum DGDA-2490 BK BMPE resin with a reported density of 0.959 kg m^{-3}. The resin was reported to have a PENT (ASTM F1473) lifetime longer than 10,000 h by The Dow Chemical Company.

The specimens were cut from the real pipe, rather than from compression molded plaques, because it has been found that the thermal history during compression molding strongly affects the fracture kinetics [13]. Kanniene et al. [18] reported that pipe field failures occur about equally in both circumferential and radial directions. In addition, Shah et al. [19] in our group showed that crack propagation in a non-standard specimen cut from real pipe can be effectively simulated using a standard compact tension specimen. Therefore, standard compact tension specimens with dimensions in accordance with ASTM D5045 were cut parallel to the radius of the pipe so that the crack propagated in the radial direction as shown in Fig. 1. A thickness of 13 mm ensured plane strain conditions and also was the limit due to the pipe dimensions. V-shaped side grooves 1 mm in depth were cut into the specimen to minimize the plane stress condition near the edge. The notch was prepared in two steps. An initial 9.5 mm cut was made with a band saw on the inner side of the pipe and a final 2.5 mm cut was achieved by pushing a fresh razor blade at a controlled speed of 1 μm s^{-1}. A fresh razor blade was used for each specimen.

Fatigue tests

Fatigue tests were performed with mechanical fatigue units equipped with a heated air chamber. The mechanical fatigue units were capable of applying a stable (±0.5 N) and accurate sinusoidal load in a fatigue loading cycle. The temperature in the chamber was maintained at 50 °C for most of the fatigue tests. The mean stress intensity, $K_{I,mean}$, defined as the average of the maximum stress intensity,

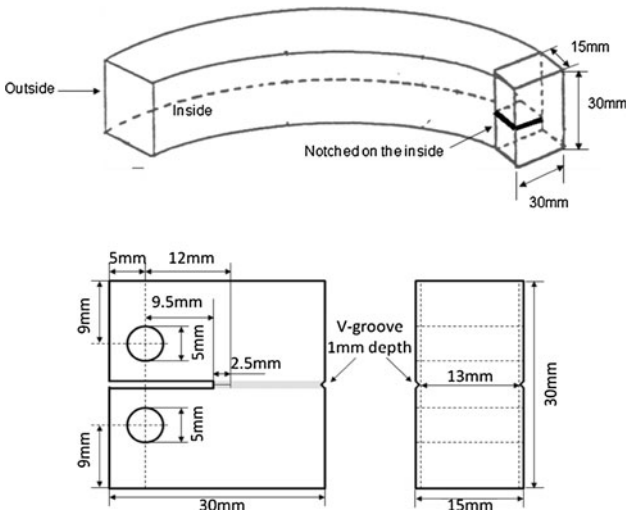

Fig. 1 Geometry of the compact tension specimens cut from the pipe wall

$K_{I,max}$, and the minimum stress intensity, $K_{I,min}$, was varied from 0.65 to 0.95 MPa $m^{1/2}$. The R-ratio, defined as $K_{I,min}/K_{I,max}$, was also varied. All the fatigue experiments were performed at a frequency of 1 Hz. The applied load, crosshead displacement and time were recorded by computer every 1000 s during the tests. A manual zoom macrolens attached to a monochrome video camera was used to observe the crack tip and to measure the crack depth during crack propagation. The camera was focused on the root membrane formed at the crack tip. The output of the camera was routed through a VCR to a black and white video monitor, and when necessary, the experiment was recorded onto a videocassette for later analysis.

Additional tests were performed at 21, 40, 50, 60, 70, 80, 90 °C. In these tests, $K_{I,mean}$ was varied from 0.75 to 0.40 MPa $m^{1/2}$ in order to conserve stepwise discontinuous crack propagation at each temperature. All of the tests were performed at a frequency of 1 Hz.

After each experiment, the fracture surfaces were examined under the optical microscope. Features were best resolved in reflection mode using normal incidence illumination. Some of the fatigue fracture surfaces were coated with 10 nm of gold and examined in a JOEL JSM-6510LV scanning electron microscope (SEM). The accelerator voltage did not exceed 10 kV in order to minimize radiation damage to the specimens.

Some specimens were fatigued for a predetermined number of cycles, removed from the fatigue unit, and sectioned using a low speed Isomet diamond knife to obtain a side view of the craze damage zone ahead of the crack tip. The sectioned pieces were coated with 10 nm of gold and viewed under a SEM in the secondary electron imaging (SEI) mode.

Mechanical tensile testing and dynamic mechanical thermal analysis

Dog bone shape specimens in accordance to the geometry of ASTM D1708 were cut from plaques compression molded directly from pipe. The plaques were rapidly cooled using the conditions that have been shown to best reproduce the crack-resistant properties of pipe [13]. 1000% strain rate was chosen for the tensile testing. The stress–strain response was determined with an MTS Alliance RT/30 testing machine. Five repetitions were done for tensile testing.

The dynamic mechanical response was determined with a Rheometrics DMA Q800 in the tensile mode. The dynamic measurement was subject to a small strain amplitude of 0.2% at a sample length of 15 mm (distance between the clamps) and A small static force of 0.01 N at a sample geometry of $15\times8\times0.2$ mm^3 (length × width × thickness) to ensure tension mode. The experiments were performed at frequencies of 0.1, 1, 10, and 50 Hz. The temperature was increased at a rate of 3 K min^{-1}.

The frequency dependence of the maximum in the tensile loss modulus E'' was used to determine the activation energy E_a of the α-relaxation according to the Arrhenius equation.

$$f(T) = Ae^{-\frac{E_a}{RT}} \tag{3}$$

$$\ln f(T) = -\frac{E_a}{R}\left(\frac{1}{T}\right) + \ln(A) \tag{4}$$

Results and discussion

Effect of R-ratio on slow crack growth

The effect of R-ratio on fatigue crack propagation at 50 °C was probed under constant $K_{I,mean} = 0.75$ MPa $m^{1/2}$. The time dependence of the maximum crosshead displacement is shown in Fig. 2 for $R = 0.1$, 0.2, and 0.3 and the corresponding fracture surfaces are shown in Fig. 3. The typical stepwise character of crack propagation, which is due to sequential formation and fracture of a crack tip damage zone, was easily observed on the crosshead displacement plot and on the fracture surface for $R = 0.1$. The plateau regions of the displacement curve corresponded to crack arrest periods, during which a craze damage zone formed to alleviate the stress concentration at the crack tip [20]. Failure of the damage zone began with fracture of the craze fibrils followed by fracture of the crack tip membrane. A sharp step in the crosshead displacement curve occurred when the membrane fractured and the crack jumped through the fractured craze to begin a new craze damage zone. Remnants of the broken membranes produced the periodic striations on the fracture surface.

When the R-ratio was increased to 0.2 or 0.3, the step jumps were not as obvious on the crosshead displacement curve and well defined striations were not as apparent on the fracture surface under $K_{I,mean} = 0.75$ MPa $m^{1/2}$. To

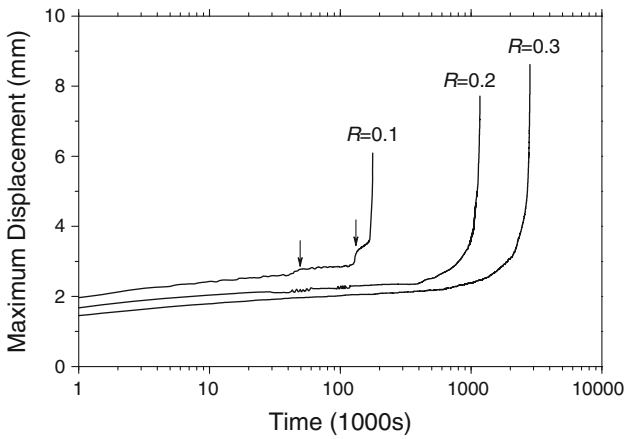

Fig. 2 Maximum crosshead displacement versus log time for fatigue tests at 50 °C and $K_{I,mean} = 0.75$ MPa $m^{1/2}$ at different R-ratios ($R = 0.1$, 0.2, 0.3)

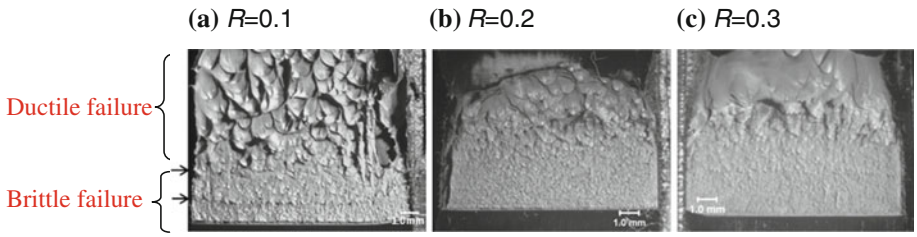

Fig. 3 Fracture surfaces of the specimens tested in Fig. 2 under $K_{I,mean} = 0.75$ MPa $m^{1/2}$ and $R = 0.1$, 0.2, and 0.3. (Only the data for the first step was used to construct modified Paris Law.)

confirm the stepwise nature of crack propagation, fatigue experiments under $K_{I,mean} = 0.75$ MPa $m^{1/2}$ and $R = 0.2$ were stopped after a prescribed number of cycles and the specimens were sectioned to obtain side views of the damage zone, Fig. 4. After about 10% of the first step lifetime (point a in Fig. 4), a typical damage zone for stepwise crack propagation in polyethylene was observed [19]. It consisted of a main craze with a continuous membrane at the crack tip. Subsidiary shear crazes emerged from the membrane region at an angle of about 30° with respect to the primary craze. The crack tip main craze had reached 80% of the first step length after about 10% of the first step lifetime. At about 90% of the craze lifetime (point b in Fig. 4) examination of the crack tip opening revealed that the membrane ahead of the crack tip had formed some elliptical holes, and voids could be seen behind the membrane. A side view confirmed that part of the craze had fractured but the membrane remained intact. After the shallow step in the displacement curve (point c in Fig. 4), the membrane was fully ruptured, the main craze was completely broken, and a new craze damage zone had begun to form. From these observations, it appeared that

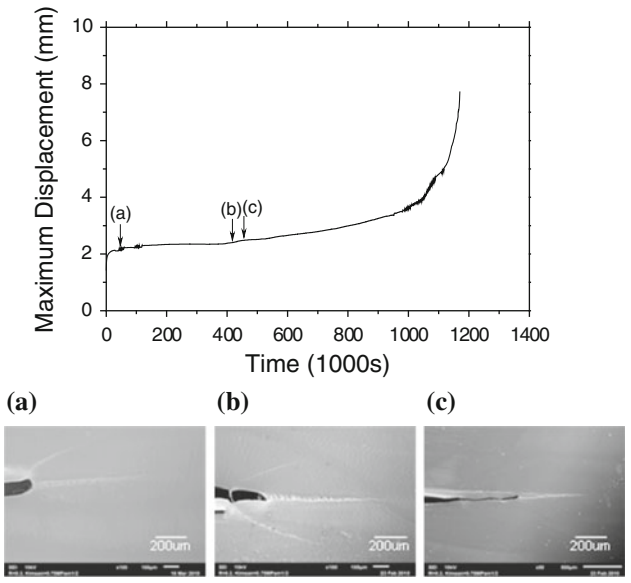

Fig. 4 Side views of the damage zone after a prescribed number of cycles for $R = 0.2$, $K_{I,mean} = 0.75$ MPa $m^{1/2}$. **a** 86,000 cycles; **b** 420,000 cycles; and **c** 470,000 cycles

the membrane and the main craze fractured concurrently. As a consequence, the stepwise propagation was not revealed as clearly in the displacement curve or on the fracture surface. The stepwise crack growth through a crack tip craze zone was similarly confirmed for all the *R*-ratios studied, Table 1. Despite the modification in fracture mode from sequential fracture of the main craze and the membrane to concurrent fracture, the damage zone, as characterized by the length of the main craze and shear crazes, followed the same dependence on loading parameters, and the crack growth rate followed the same kinetics [15]. The length of the craze damage zone as measured from the fracture surfaces and the side views was about 1 mm for *R*-ratios of 0.1, 0.2 and 0.3 under $K_{I,mean} = 0.75$ MPa $m^{1/2}$.

An additional series of fatigue experiments was performed at constant $K_{I,max} = 1.17$ MPa $m^{1/2}$ and *R*-ratios of 0.1, 0.2, and 0.3, Fig. 5. Both the first step lifetime and the overall lifetime increased significantly with increasing *R*-ratio. The step jumps were clearly visible in the displacement curve for $R = 0.1$. However, the step jumps were not as apparent in curves for *R*-ratios of 0.2 and 0.3. Nevertheless, it was confirmed from the fracture surfaces and side views of the damage zone that the stepwise crack propagation mode was conserved for all *R*-ratios under constant $K_{I,max} = 1.17$ MPa $m^{1/2}$.

Increasing K_I resulted in ductile fracture ($R = 0.1$, $K_{I,mean} = 0.85$, 0.95 MPa $m^{1/2}$) [21], or crack propagation through a shear craze (R=0.2, $K_{I,mean} = 0.80$, 0.84, 0.91 MPa $m^{1/2}$) [15], instead of stepwise propagation through a main craze, Table 1. Fatigue under lower *K* or higher *R*-ratio resulted in impractically long lifetimes. Data for *R*-ratios of 0.1, 0.2, 0.3, and 0.4 obtained at intermediate *K* values where stepwise crack propagation was observed were used to predict fatigue failure at higher *R*-ratios and creep failure ($R = 1$) in BMPE.

Analysis of experiments performed under constant $K_{I,max}$ and constant $K_{I,mean}$ revealed that the crack jump length was determined primarily by $K_{I,mean}$. The dependence of damage zone length on $K_{I,mean}$ rather than on $K_{I,max}$ resulted from the time scale of craze growth. The time for completion of a single fatigue loading cycle was negligible compared to the duration of craze growth. Therefore, the stress that controlled the craze length was the average stress, i.e., the mean stress.

Table 1 Experimental matrix that was designed to get the stepwise mechanism in order to construct Paris plot at different *R*-ratios

R-ratio	$K_{I,mean}$ (MPa $m^{1/2}$)	$K_{I,max}$ (MPa $m^{1/2}$)	$K_{I,min}$ (MPa $m^{1/2}$)	ΔK_I (MPa $m^{1/2}$)	Fracture mode	First step length (mm)	First step lifetime ($\times 10^3$ s)	First step crack growth rate ($\times 10^{-5}$ mm s^{-1})	Overall lifetime ($\times 10^3$ s)
0.1	0.65	1.18	0.12	1.06	Stepwise	0.80	204	0.391	450 ± 20
0.1	0.70	1.27	0.13	1.14	Stepwise	0.85	163	0.522	285
0.1	0.75	1.36	0.14	1.23	Stepwise	1.07	140	0.762	180 ± 5
0.1	0.80	1.46	0.15	1.31	Stepwise	1.10	104	1.055	147
0.1	0.85	1.55	0.16	1.39	Ductile	–	–	–	62
0.1	0.95	1.73	0.17	1.56	Ductile	–	–	–	10
0.2	0.65	1.08	0.22	0.86	Stepwise	1.00	861	0.116	2229
0.2	0.70	1.17	0.23	0.94	Stepwise	1.10	665	0.165	1740 ± 82
0.2	0.75	1.25	0.25	1.00	Stepwise	1.00	454	0.220	1165
0.2	0.80	1.33	0.27	1.06	Ductile	–	–	–	1130 ± 75
0.2	0.84	1.40	0.28	1.12	Ductile	–	–	–	927
0.2	0.91	1.52	0.30	1.22	Ductile	–	–	–	731
0.3	0.65	0.92	0.28	0.64	Stepwise	0.70	1437	0.045	X
0.3	0.70	1.07	0.32	0.75	Stepwise	0.90	1290	0.070	3618
0.3	0.75	1.15	0.35	0.81	Stepwise	1.00	1059	0.094	2824
0.3	0.84	1.29	0.39	0.90	Ductile	–	–	–	2477
0.4	0.70	1.00	0.40	0.60	Stepwise	0.80	2500	0.0312	X
0.4	0.75	1.07	0.43	0.64	Stepwise	0.80	1980	0.0405	X

X experiment was stopped before the sample was completely ruptured

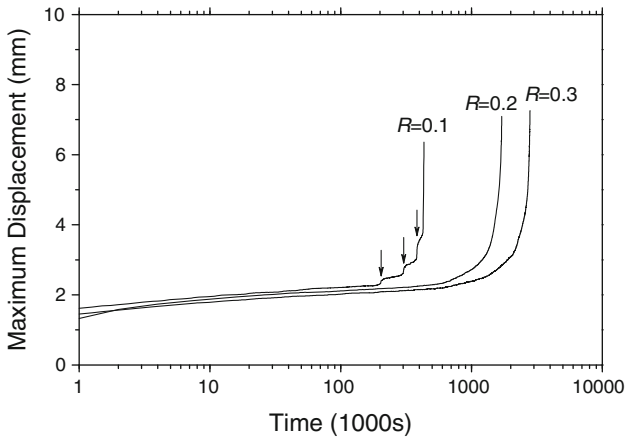

Fig. 5 Maximum crosshead displacement versus log time for fatigue tests at 50 °C and $K_{I,max} = 1.17$ MPa $m^{1/2}$ at different *R*-ratios ($R = 0.1, 0.2, 0.3$)

The Dugdale model is widely used to relate craze zone length to the applied stress intensity factor

$$l = \frac{\pi}{8}\frac{K_I^2}{\sigma_y^2} \tag{5}$$

where K_I is the stress intensity factor for mode I and σ_y is the yield stress which depends on strain rate and temperature. Because the craze length was controlled by $K_{I,mean}$, this quantity was used to represent the stress intensity in Eq. 1. The step length *l* was shown to be proportional to $K_{I,mean}^2$ for all *R*-ratios studied, Fig. 6. From the linear fit in Fig. 6, the yield stress for BMPE at 50 °C was 14.6 MPa, which agreed well with the measured yield stress of 16 MPa.

Kinetics of fatigue crack propagation

The crack growth rate (d*a*/d*t*) for stepwise crack propagation is conventionally calculated from the step jump length

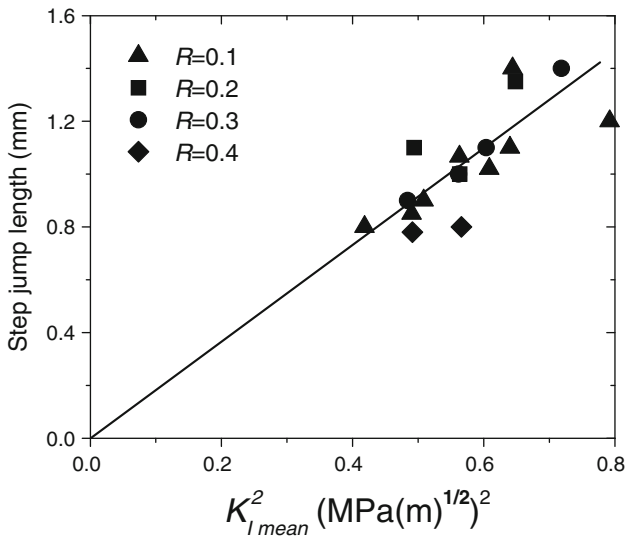

Fig. 6 Effect of $K_{I,mean}$ on the first step jump length for fatigue tests at $R = 0.1, 0.2, 0.3$, and 0.4

(da) and the duration of the step jump (dt). For a given R-ratio, the dependence of crack growth rate in fatigue on the stress intensity factor is usually described by the Paris relation

$$\frac{da}{dt} = A\Delta K_I^m \tag{6}$$

where $\Delta K_I = K_{I,max} - K_{I,min}$ in the fatigue cycle and the prefactor A and the power m are material constants. In numerous studies, the power m was determined to be independent of temperature and R-ratio, and equal to 4 for polyethylene resins [15–17]. The prefactor A depends on the specific resin and is a measure of the resistance to fatigue crack propagation. A plot of log (da/dt) versus log ΔK_I for the various R-ratios shows that the fatigue data conform to Eq. 4 with $m = 4$, Fig. 7a. However, the Paris relation and other Paris-type relations where stress intensity factor is represented by ΔK_I are not applicable to creep testing where $\Delta K_I = 0$.

For fatigue at constant temperature and frequency, there are five loading variables that can be used to describe the fatigue cycle: R-ratio, ΔK_I, $K_{I,max}$, $K_{I,min}$, and $K_{I,mean}$, however, only two of these are independent. Because the Paris relation relates crack growth rate only to ΔK_I, one of the other variables, usually the R-ratio, is held constant. In order to express data for various R-ratios in a form that could be extrapolated to creep loading ($R = 1.0$), the dependencies on $K_{I,max}$ and $K_{I,mean}$ were determined independently. Figure 8a shows log (da/dt) for the first step jump plotted versus log $K_{I,max}$ for $K_{I,mean} = 0.75$ MPa m$^{1/2}$. A linear relationship was obtained over the entire range of $K_{I,max}$ with a slope of 12.5. Increasing $K_{I,max}$ decreased dt without affecting da, and therefore da/dt was strongly dependent on $K_{I,max}$. Similarly, the effect of $K_{I,mean}$ was obtained by plotting log (da/dt) versus log $K_{I,mean}$ for tests under $K_{I,max} = 1.17$ MPa m$^{1/2}$, Fig. 8b. Again, a linear relationship was observed over the entire range of $K_{I,mean}$, in this case with a slope of −8.5. Increasing $K_{I,mean}$

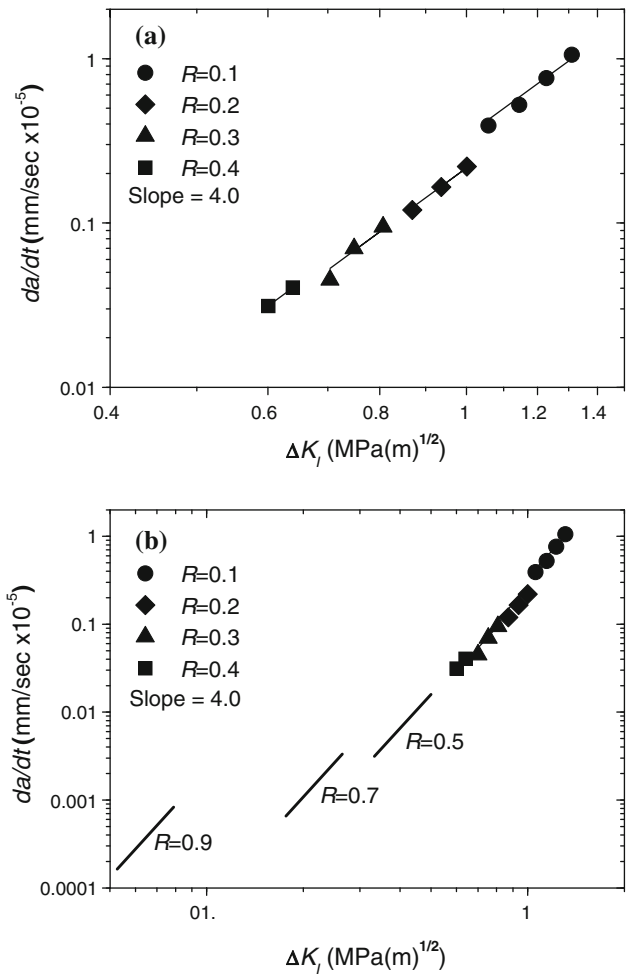

Fig. 7 Paris plots of crack growth rate (da/dt versus ΔK_I) at 50°C for different R-ratios. **a** Measured values; and **b** crack growth rate for higher R-ratios calculated from Eq. 11

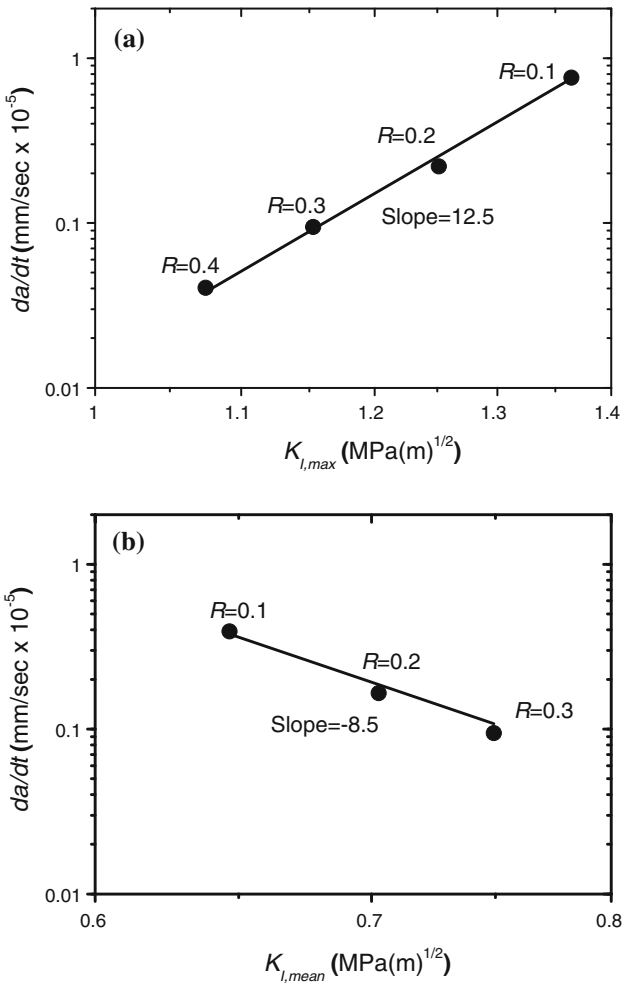

Fig. 8 Formulation of the modified Paris plot based on the empirical dependence of crack growth rate on **a** $K_{I,max}$ (constant $K_{I,mean} = 0.75$ MPa m$^{1/2}$); and **b** $K_{I,mean}$ (constant $K_{I,max} = 1.17$ MPa m$^{1/2}$)

increased the step jump length (da), but also increased the step jump lifetime (dt). The net result was that the crack growth rate was less dependent on $K_{I,mean}$ than on $K_{I,max}$.

The dependencies of crack growth rate on $K_{I,max}$ and $K_{I,mean}$ led to a power law relationship for crack growth rate

$$\frac{da}{dt} = BK_{I,max}^{12.5}K_{I,mean}^{-8.5} \quad (7)$$

where the prefactor B is a material constant that depends on temperature and frequency. In creep ($K_{I,max} = K_{I,mean} = K_I$) Eq. 7 reduces to the conventional Paris relation for creep in polyethylene as given by

$$\frac{da}{dt} = BK_I^4 \quad (8)$$

For convenience, Eq. 7 was reformulated as

$$\frac{da}{dt} = B'K_{I,max}^4(1+R)^{-8.5} \quad (9)$$

where $B' = 2^{8.5}B$. Equation 9 follows a general form that has been observed for other polyethylene resins [14, 15, 17]

$$\frac{da}{dt} = B'K_{I,max}^4(1+R)^n \quad (10)$$

where the prefactor B' and the power n depend on the specific resin. Although B' depends on temperature, the power n appears to be independent of temperature [15, 17]. The term $(1+R)^n$ is a measure of the sensitivity of the resin to R-ratio in fatigue. The prefactor B' is a temperature-dependent material parameter. In creep, Eq. 10 reduces to Eq. 8.

All the fatigue data for BMPE are plotted according to Eq. 7 in Fig. 9. The data followed a straight line fit with a slope of 1. The prefactor B' extracted from the linear regression was 5.0×10^{-6} mm m^2 s^{-1} MPa^{-4}, which gave a creep prefactor $B = 1.4 \times 10^{-8}$ mm m^2 s^{-1} MPa^{-4}. The Paris plots for R-ratios as high as 0.9 were calculated for $m = 4$ by rearranging Eq. 9 using the extracted value of B'

$$\frac{da}{dt} = \left[B'(1-R)^{-4}(1+R)^{-8.5}\right](\Delta K_I)^4 \quad (11)$$

Although the Paris plots for lower R-ratios appeared to follow a single linear relationship, substantial deviation was predicted as the R-ratio increased approaching creep ($R = 1$), Fig. 7b.

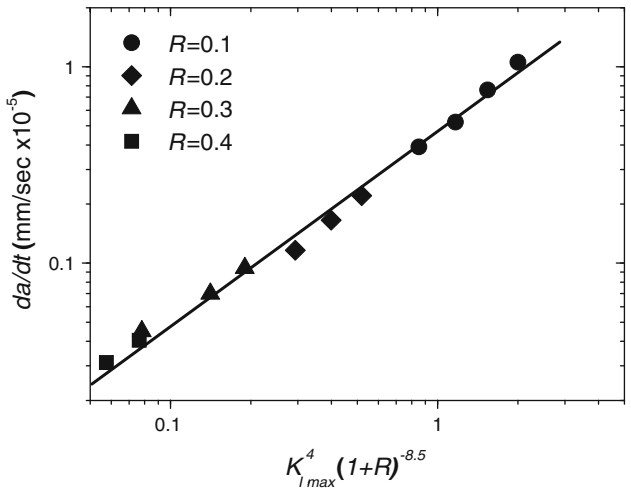

Fig. 9 Fit of BMPE test data at 50 °C to the modified Paris law

Temperature dependence of the prefactor B'

The temperature dependence of the crack growth rate is contained in the prefactor B'. The crack growth rate was obtained at various temperatures between 21 and 90 °C using values of $K_{I,mean}$ and R-ratio that produced stepwise crack propagation, Table 2. The prefactor B' was calculated from Eq. 9 using the crack speed (da/dt) of the first crack jump and the fatigue loading conditions. An Arrhenius plot of ln B' versus $1/T$ was constructed, Fig. 10. The data were described by two straight lines with a slope change at 67 °C. The extracted activation energies were 89 kJ mol^{-1} for the high temperature region and 22 kJ mol^{-1} for the low temperature region. A similar slope change was observed in the temperature dependence of B' for a conventional medium density polyethylene pipe resin (MDPE) with similar activation energies of 125 kJ mol^{-1} and 25 kJ mol^{-1} [15]. The high temperature process was related to the α-relaxation. The activation energy obtained from Fig. 10 correlated with the activation energy of the α-relaxation, and the temperature of the slope change in the Arrhenius plot coincided with the temperature of the α-relaxation as defined by DMTA. It is noteworthy that both the slope change and the α-relaxation temperature for BMPE occurred at a temperature about 12 °C higher than for MDPE. Below 67 °C, a much lower activation energy was obtained. The low temperature process was ascribed to the amorphous entanglement network.

For the lifetime prediction, the lifetime depends on the pipe wall thickness and the stress intensity that the pipe is subject to. If the pipe wall thickness and the stress intensity are known, then the lifetime of the bimodal pipe can be calculated using Eq. 1 (a modified Paris Law). The modified Paris Law parameters and the creep prefactors for various polyethylene resins are compared in Table 3. By comparing the creep factors, B, for different pipes, the relative performance of those pipes can be ranked. The comparison of n indicated that the dependence of fatigue on R-ratio as expressed in the parameter n became stronger as the resin became more resistant to slow crack growth. A qualitative comparison made in a previous study also suggested that fatigue was more effective in accelerating

Table 2 Experimental matrix for temperature dependence of stepwise crack growth

Temperature (°C)	R-ratio	$K_{I,mean}$ (MPa $m^{1/2}$)	$K_{I,max}$ (MPa $m^{1/2}$)	First step length (mm)	First step lifetime ($\times 10^3$s)	Prefactor B' (mm m^2 s^{-1} MPa^{-4} $\times$ 10^5)	Yield stress[a] (MPa)
21	0.1	0.75	1.36	0.59	185	0.20	19.3
21	0.1	0.85	1.55	0.72	139	0.20	20.8
21	0.1	1.00	1.82	1.01	104	0.19	19.7
40	0.1	0.75	1.36	0.82	172	0.31	16.4
50	0.1	0.75	1.36	0.80	204	0.48	14.6
60	0.1	0.65	1.18	0.96	203	0.56	13.1
70	0.1	0.50	0.91	0.72	275	0.86	11.7
80	0.1	0.40	0.73	0.67	310	1.77	9.7
90	0.1	0.40	0.73	0.93	170	4.33	8.2

[a] Calculated from Eq. 5

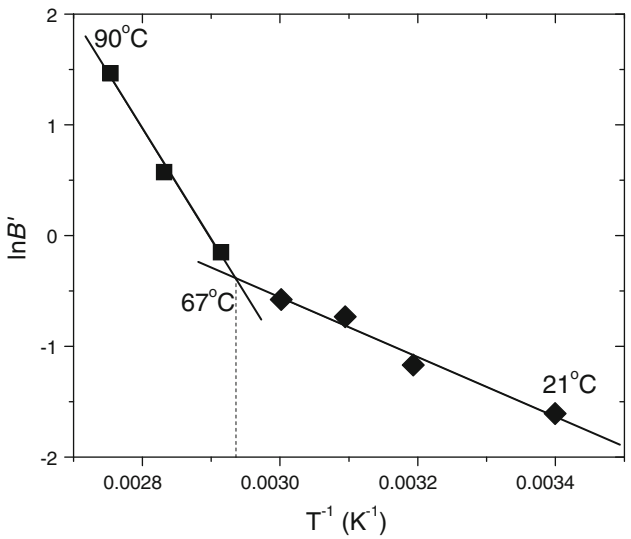

Fig. 10 Arrhenius plot of the temperature-dependent prefactor B' for BMPE

slow crack growth in resins with higher creep resistance [13]. Our longest experiment on first step lifetime at the condition of $R = 0.4$, $K_{I,mean} = 0.70$ MPa $m^{1/2}$ for BMPE took about 1 month (7,00 h). The PENT test would have taken around a year or more (10,000 h) to make this prediction.

The creep crack growth rate in BMPE is predicted to be more than an order of magnitude slower than in MDPE. The structural origin of the fracture toughness of polyethylene is thought to reside in the interlamellar tie molecules. Upon loading, the tie molecules stretch as they take up the applied stress and form taut links between crystals. This leads to local yielding and breakup of the crystals, and formation of highly oriented fibrils. These fibrils form the damage zone at the crack tip. For creep and fatigue, fibril fracture is ascribed primarily to chain disentanglement, which requires chain slippage and pullout [13]. Both the density of tie molecules and the rate of chain pullout depend on the molecular weight and the branch content. As molecular weight increases, more tie chains form and more time is required to disconnect a tie chain from a crystal. Introducing chain branches dramatically improves the fracture toughness. Short branches act as protrusions along the chain that significantly hamper chain disentanglement. By impeding a tie chain from sliding through a crystal, the short chain branches considerably increase the disentanglement time. In conventional polyethylene copolymers, the chain branch content decreases with molecular weight. Thus, the branch content is highest in the chains that are least likely to be involved in intercrystalline links. One way to make the branches more efficient is to redistribute them to the high molecular weight chains. This approach is

Table 3 Comparison of modified Paris law and creep factor for different PEs (HDPE, MDPE, and BMPE)

Generalized Modified Paris Law: $\frac{da}{dt} = B' K_{I,max}^{m} (1+R)^{n}$

	Test T (°C)	m	n	B' (mm m^2 s^{-1} MPa^{-4} $\times$ 10^5)	Creep prefactor $B = B'2^n$ (mm m^2 s^{-1} MPa^{-4} $\times$ 10^5)	Reference
BMPE	50	4	−8.5	0.48	0.0013	
MDPE	50	4	−6.0	1.7	0.026	[17]
BMPE	21	4	−8.5	0.20	0.00055	
MDPE	21	4	−6.0	0.72	0.011	[15]
HDPE	21	4	−0.5	0.40	0.28	[16]

realized in BMPE. The lower molecular weight chains are essentially homopolymer. They increase the crystallinity, thereby providing more crystalline anchors for the tie molecules. The higher molecular weight copolymer chains provide the tie chains that link the crystals. The short chain branches hamper slippage and pullout.

Conclusions

The exceptionally high resistance of modern BMPE pipe resins to slow crack growth challenges the practicality of conventional creep failure tests for predicting the service lifetime. Short-term fatigue testing is another approach to predicting long-term creep performance. The fatigue failure time can be substantially shorter than the failure time in standard creep tests especially for resins that exhibit a high resistance to slow crack growth. This study was undertaken to determine whether a fatigue-to-creep correlation previously developed for an earlier generation of pipe resins is applicable to BMPE pipe resins, and to ascertain whether a lifetime prediction can be obtained within a reasonable time period. The stepwise mechanism of fatigue crack propagation at 50 °C was verified and the crack growth rate was related to the maximum stress and R-ratio by a power law relation. The dependence on R-ratio was a measure of the fatigue acceleration. Comparison with results for other polyethylene resins indicated a stronger dependence on R-ratio as the resin became more resistant to slow crack growth. Thus, fatigue was more effective in accelerating slow crack growth in resins with higher creep resistance. The temperature dependence of slow crack growth followed an Arrhenius relation with a change in slope at 67 °C. The change in slope indicated that extrapolation of creep behavior at temperatures above the α-relaxation to ambient temperature requires considerable caution.

References

1. Hubert L, David L, Séguéla R, Vigier G, Degoulet C, Germain Y (2001) Polymer 42:8425
2. Hubert L, David L, Séguéla R, Vigier G, Corfias-Zuccalli C, Germain Y (2002) J Appl Polym Sci 84:2308
3. Rose LJ, Channell AD, Frye CJ, Capaccio G (1994) J Appl Polym Sci 54:2119
4. Shah A, Stepanov EV, Cappaccio G, Hiltner A, Baer E (1998) J Polym Sci B 36:2355
5. United States Patent, US 7, 193, 017 B2, 3/20/2009 Tae Hoon Kwalk, Univation Technology, LLC
6. Lu X, Zhou Z, Brown N (1997) Polym Eng Sci 37:1896
7. Zhou Z, Brown N (1996) Polym Test 15:549
8. Brown N, Zhou ZJ (2005) Plast Rubber Compos 34:289
9. Raise the bar on polyethylene pipe performance: Dow® Continuum™ polyethylene resins for PE4710/PE100 pipe. http://www.dow.com. Accessed 14 June 2010
10. Huang YL, Brown N (1988) J Mater Sci 23:3648. doi:10.1007/BF00540508
11. Strebel JJ, Moet A (1992) Int J Fract 54:21
12. Choi BH, Balika W, Chudnovsky A, Pinter G, Lang RW (2009) Polym Eng Sci 49:1421
13. Shah A, Stepanov EV, Klein M, Hiltner A, Baer E (1998) J Mater Sci 33:3313. doi:10.1023/A:1013229128686
14. Parsons M, Stepanov EV, Hiltner A, Baer E (1999) J Mater Sci 34:3315. doi:10.1023/A:1004616728535
15. Parsons M, Stepanov EV, Hiltner A, Baer E (2000) J Mater Sci 35:2659. doi:10.1023/A:1004789522642
16. Parsons M, Stepanov EV, Hiltner A, Baer E (2000) J Mater Sci 35:1857. doi:10.1023/A:1004741713514
17. Ayyer R, Hiltner A, Baer E (2007) J Mater Sci 42:7004. doi:10.1007/s10853-006-1108-2
18. Kanninen M, Popelar C, Tweedy L (1991) 12th plastic fuel gas pipe symposium proceedings. Boston, Mass, p 113
19. Shah A, Stepanov E, Hiltner A, Baer E (1997) Int J Fract 84:159
20. Parsons M, Stepanov EV, Hiltner A, Baer E (2001) J Mater Sci 36:5747. doi:10.1023/A:1012935517866
21. Brown N, Ward I (1983) J Mater Sci 18:1405. doi:10.1007/BF01111960